Polymer 50 (2009) 1251–1256

Contents lists available at ScienceDirect

Polymer

journal homepage: www.elsevier.com/locate/polymer

Interface structure of poly(ethylene terephthalate)/silica nanocomposites

Xiayin Yao [a], Xingyou Tian [a,b], Dinghai Xie [c], Xian Zhang [a], Kang Zheng [a], Jun Xu [d], Gangzhao Zhang [c], Ping Cui [a,b,*]

[a] Key Laboratory of Materials Physics, Institute of Solid State Physics, Chinese Academy of Sciences, Hefei 230031, China
[b] Ningbo Institute of Material Technology & Engineering, Chinese Academy of Sciences, Ningbo 315040, China
[c] Department of Chemical Physics, University of Science and Technology of China, Hefei 230026, China
[d] State Key Laboratory of Magnetic Resonance and Atomic and Molecular Physics, Wuhan Institute of Physics and Mathematics, Chinese Academy of Sciences, Wuhan 430071, China

ARTICLE INFO

Article history:
Received 28 June 2008
Received in revised form
12 December 2008
Accepted 9 January 2009
Available online 14 January 2009

Keywords:
PET-grafted-silica nanocomposites
Branching
Lightly crosslinking

ABSTRACT

The interface structure of the poly(ethylene terephthalate) (PET)/silica nanocomposites was characterized by Fourier transform infrared and solid-state nuclear magnetic resonance. Our study reveals that PET chains are grafted onto the surface of silica nanoparticles, and they form branched and lightly crosslinking structures during the polycondensation. Gel permeation chromatography measurements indicate that the grafted PET chains have a lower molecular weight and broader distribution. Furthermore, a model has been developed to elucidate the interaction of an entanglement network between silica and PET chains that lead to enhancements of G', G'' and η^* values of PET/2 wt% silica nanocomposites.

© 2009 Published by Elsevier Ltd.

1. Introduction

The study of polymer/inorganic nanocomposites is of great interest to both industry and academy because they exhibit significantly improved properties in comparison with conventional materials, including electrical/magnetic properties, mechanical properties, thermal stability, gas barrier, fire retardence and so on [1–5]. Most nanocomposites reported up to now are usually prepared by physisorption or covalent attachment of polymer chains to the surface of nanoparticles. Due to the poor adhesion, the nanocomposites exhibit limited improvement in their properties. In contrast, when polymer chains are tethered to nanoparticle surface by covalent bond, a strong adhesion between nanoparticle and polymer matrices can be resulted. Generally, covalent attachment can be achieved by the so-called "grafting to" or "grafting from" procedure. In the former, end-functionalized polymers are grafted to the nanoparticle surface. Because the already grafted polymer chains sterically shield the reactive sites on the surface, the grafting density is low. In the latter, the initiator is attached on the surface so that the polymer chains form in situ, leading to a high grafting density.

In recent years, a number of works about chemically grafting of nanoparticle surface have been reported [6,7]. And in most cases prior surface functionalization of nanoparticles is required [8–13]. One of the most used procedures is the controlled/"living" polymerization because it can well control the molecular weight, molecular weight distribution and structure of the grafted polymers [14–23]. Patten and co-workers [14] have prepared well-defined polymer–silica nanoparticle hybrids via atom transfer radical polymerization (ATRP) of methyl methacrylate and styrene. However, some disadvantages of ATRP may be that control over the polymerization is obtained at the cost of a decreased polymerization rate and the catalyst is also difficult to remove. So far, only a few studies deal with covalent attachment of polymer chains to the nanoparticle surface via polycondensation [24,25].

Poly(ethylene terephthalate) (PET), an important commercial product, has been widely used in fields of fibers and nonfibers due to its low cost and good properties such as chemical resistance, thermal stability, etc. However, the low crystallization rate, low thermal distortion temperature and low modulus limit its applications in more fields. Recently, in situ polymerization has been widely used and proved to be an effective way to prepare high performance nanocomposites [26–33]. To improve PET properties, PET/inorganic nanocomposites have also been prepared by in situ polymerization [34–38]. However, the grafting mechanism and the structure of the nanocomposites are not well understood.

In our previous work, we have synthesized PET/silica nanocomposites with homogeneously dispersed silica nanoparticles by

* Corresponding author. Key Laboratory of Materials Physics, Institute of Solid State Physics, Chinese Academy of Sciences, Hefei 230031, China. Tel.: +86 551 5591410; fax: +86 551 5591434.
E-mail address: pcui@issp.ac.cn (P. Cui).

0032-3861/$ – see front matter © 2009 Published by Elsevier Ltd.
doi:10.1016/j.polymer.2009.01.008

in situ polymerization of terephthalic acid (TPA), ethylene glycol (EG) and pure silica [39]. Higher molecular weight of the PET/silica nanocomposites has been reached by solid-state polymerization and the obtained nanocomposites are produced to fibers through melt-spinning. The mechanical properties and heat-shrinkage of the fibers made of these nanocomposites are greatly improved in comparison with those of pure PET fibers. In the present study, we have investigated the interface structure of the PET/silica nanocomposites. It can help us to design high performance materials.

2. Experimental

2.1. Materials

Terephthalic acid and antimony acetate (as catalyst) were kindly supplied by Changzhou Huayuan Radics Co., Ltd. (China). An aqueous solution of silica particles (about 12 nm in diameter, 30 wt%) was obtained from Zhoushan Mingri Nano-company (Zhengjiang, China). Ethylene glycol, phenol, tetrachloroethane, hydrogen fluoride, trifluoroacetic acid, methanol and absolute ethanol were purchased from Shanghai Chemical Reagent Corp. (China). All the reagents were used without further purification.

2.2. Preparation of PET-grafted-silica nanocomposites

The details of pure PET and PET/2 wt% silica nanocomposites can be found elsewhere [39]. The procedure of successive centrifugation/redissolved cycles was used to isolate the PET-grafted-silica nanocomposites from the PET/2 wt% silica nanocomposites containing ungrafted PET. The PET/2 wt% silica nanocomposites were dissolved in mixed solvents of phenol and tetrachloroethane (1/1, w/w) and there was no insoluble portion found. The solution was centrifuged at 10 000 rpm for at least 30 min. Afterwards, the solid material obtained was repeatedly redissolved in the above mixture of solvents and separated again by centrifugation. The supernatant solutions were dropwise added to a 10–15 times excess of methanol and the precipitate, i.e. free PET, was collected by centrifugation. This centrifugation/redissolved procedure was repeated until no more precipitate formed when the supernatant liquid was dropwise added to methanol, indicating that no ungrafted and physisorbed PET could be removed. The resulting solid material (i.e. PET-grafted-silica nanocomposites or hybrid nanoparticles) and free PET were washed extensively with absolute ethanol to remove the solvent and dried to constant weight at 80 °C under vacuum.

2.3. Cleavage of the grafted PET from PET-grafted-silica nanocomposites

PET-grafted-silica nanocomposites were introduced into mixed solvents of phenol and tetrachloroethane (1/1, w/w), and a 5% aqueous hydrogen fluoride solution was added. The mixture was stirred overnight at room temperature. The organic layer was removed, and the polymer (i.e. grafted PET) was isolated by precipitation from methanol. Then the grafted PET was collected by centrifugation, washed extensively with absolute ethanol and dried to constant weight at 80 °C under vacuum.

2.4. Characterization

Fourier transform infrared (FT-IR) spectra were recorded on a Nicolet MAGNA-IR 750 spectrometer over the range 4000–400 cm^{-1} using KBr pellets. ^{29}Si single pulse excitation magic angle spinning (SPE MAS) solid-state NMR experiments were performed at a static field of 9.4 T on a Varian Infinitypulse-400 spectrometer with resonance frequencies of 79.5 MHz. A Chemagnetics 7.5 mm triple resonance MAS probe was employed to acquire ^{29}Si NMR spectra with a spinning rate of 5 kHz. The 90° pulse width was measured to be 5.5 μs. Repetition time of 60 s for ^{29}Si SPE MAS experiments was used to obtain a quantitative measurement of the ^{29}Si signals. Thermogravimetric analyses (TGA) were performed in air at a heating rate of 10 °C min^{-1} from room temperature to 800 °C using a Perkin–Elmer Pyris-1 thermal analyzer. Transmission electron microscopy (TEM) experiments were performed on an FEI Tecnai G^2 F20 transmission electron microscopy at an accelerating voltage of 200 kV. The PET-grafted-silica nanocomposites were embedded in epoxy and cut into 80–100 nm thick slices using an ultramicrotome with a diamond knife. X-ray diffraction (XRD) patterns were obtained on a Philips model X' pert PRO X-ray diffractometer system, operating at a voltage of 40 kV and a current of 40 mA and scanning from 10 to 40°. The molecular weights of PET were measured by gel permeation chromatography (GPC) using a Polymer Laboratories PL-GPC 220 Chromatograph at 40 °C. PET was firstly dissolved in o-chlorophenol with a concentration of 10 mg/mL and then diluted into 1 mg/mL by chloroform for GPC analysis. Chloroform was used as eluent at a flow rate of 1.0 mL/min and monodisperse polystyrenes were used as the standards. Laser light scattering (LLS) measurements were conducted on an ALV/DLS/SLS-5022F spectrometer with a multi-τ digital time correlation (ALV5000) and a cylindrical 22 mW UNIPHASE He–Ne laser ($\lambda_0 = 632$ nm) as the light source at 298 K. Grafted PET was dissolved in trifluoroacetic acid [40] with a concentration of 10 mg/mL due to low molecular weight and was filtered through a 0.2 μm Whatman PTFE filter to remove dust before the LLS experiments. The hydrodynamic radius (R_h) and hydrodynamic radius distribution $f(R_h)$ were determined by dynamic LLS [41,42]. Dynamic rheological measurements were performed with a rotational rheometer (Physica MCR301, Anton Paar, Germany) using a 25 mm diameter parallel plate of 1.0 mm gap at 270 °C in a nitrogen atmosphere. The measurements were carried out in an oscillatory shear mode and frequency sweeps were performed from 0.2 to 500 rad/s at a strain of 10% which was shown within the linear viscoelastic region for these materials.

3. Results and discussion

Fig. 1 shows the FT-IR spectra of pure PET, silica and PET-grafted-silica nanocomposites. It can be seen that the FT-IR spectrum of pure PET (Fig. 1a) exhibits an important number of bands, among which those of the most characteristic can be assigned as follows

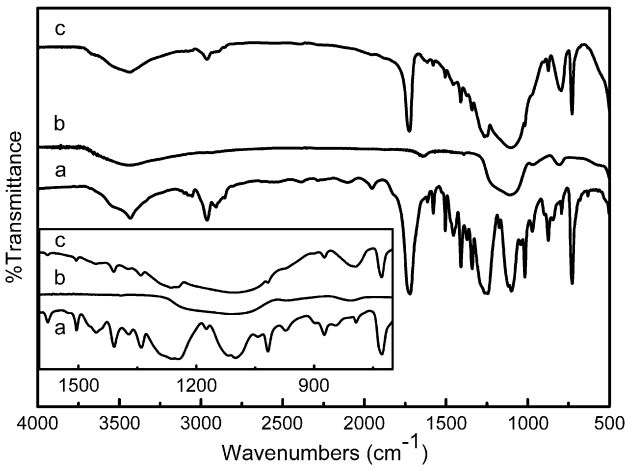

Fig. 1. FT-IR spectra for (a) pure PET, (b) silica and (c) PET-grafted-silica nanocomposites.

[43,44]: the broad bands around 3556 and 3432 cm^{-1} are attributed to the hydrogen atoms in the carboxyl end groups and stretching of ethylene glycol end groups, respectively; the band at 1720 cm^{-1} is characteristic of the C=O stretching vibration in the ester carbonyl group; the bands at 1577, 1504, 1409, 1018 cm^{-1} and 874, 727 cm^{-1} are due to in-plane and out-of-plane vibrations of the benzene rings; and the bands around 1270 and 1100 cm^{-1} result from vibrations of the ester group. Also, the characteristic bands around 3430 and 1110 cm^{-1} in Fig. 1b can be ascribed to the hydroxyl groups and the Si–O bonds of silica [25]. From the spectrum of PET-grafted-silica nanocomposites (Fig. 1c), it can be clearly seen that it consist of PET and silica because all the absorbencies correspond to PET and silica. Since the repeated cycles of centrifugation/redissolved procedure are employed to remove ungrafted and physisorbed PET, the appearance of both absorption bands of PET and silica (Fig. 1c) gives evidence for the reaction among the surface hydroxyl groups of silica and monomers of PET, i.e. TPA and EG and indicates that some PET chains have been grafted onto silica through chemical bonding rather than physical absorption. Furthermore, comparing the spectrum of PET-grafted-silica nanocomposites (Fig. 1c) with that of pure PET (Fig. 1a), the characteristic band around 1100 cm^{-1} is broadened, which is due to the overlap with the strong absorption of silica.

To further confirm the covalent attachment of PET chains to the silica surface, we also studied the PET-grafted-silica nanocomposites by solid-state NMR. Fig. 2 shows the ^{29}Si SPE MAS NMR spectra of silica and PET-grafted-silica nanocomposites. And ^{29}Si chemical shift assignments for silica and PET-grafted-silica nanocomposites are listed in Table 1. It can be seen that the silica spectrum (Fig. 2a) shows Q^3 [$(Si–O)_3Si–OH$] and Q^4 [$Si(Si–O)_4$] signals centered at −104 ppm and −114 ppm, indicating silicon atoms surrounded by one silanol group and zero silanol group [45], respectively. The Q^2 [$(Si–O)_2Si–(OH)_2$] signal at −94 ppm, which is attributed to the geminal silanols, is not shown due to its low abundance. In the spectrum of PET-grafted-silica nanocomposites (Fig. 2b), Q^4 peak can be easily observed but Q^3 peak is undiscernible. The decrease of intensity of the Q^3 peak is the direct evidence for the reaction among silica and monomers of PET.

Actually, the surface chemistry of silica has been widely surveyed [46]. Iler [47] emphasized the behavior of the silanol groups on the surface, especially their dehydration and chemical

Table 1
^{29}Si chemical shift assignments for silica and PET-grafted-silica nanocomposites.

Samples	Silicon atoms	Chemical shift (ppm)
Silica	Q^3 [$(Si–O)_3Si–OH$]	−104
	Q^4 [$Si(Si–O)_4$]	−114
PET-grafted-silica nanocomposites	Q^3 [$(Si–O)_3Si–OH$]	Undiscernible
	Q^4 [$Si(Si–O)_4$]	−114

interaction including esterification and chemisorption of organic molecules. In this study, after TPA and EG reacted with the silanol groups on the surface, PET chains grew on the nanoparticle surface.

The amount of PET grafted onto the surface of silica was determined by TGA. The weight loss curves for grafted PET, silica and PET-grafted-silica nanocomposites are presented in Fig. 3b, c and d, respectively. Analysis of these curves demonstrates that the fraction of grafted PET is 38.8 wt%. The surface grafting of a polymer onto inorganic fillers is known to be very effective at improving the dispersability in polymer matrices [48]. Indeed, the silica is homogeneously dispersed in PET matrix [39]. Fig. 4 shows the TEM micrograph of PET-grafted-silica nanocomposites. Clearly, the hybrid nanoparticles unaggregate after isolated from PET/2 wt% silica nanocomposites. The average diameter of the hybrid nanoparticles slightly varies in comparison with the as-received silica.

An interesting phenomenon is that the PET-grafted-silica nanocomposites cannot be dissolved in the mixed solvents again after dried at 80 °C under vacuum, though no 'insoluble residue' [25] has been found in PET/2 wt% silica nanocomposites. Generally, it is difficult to dissolve PET with high molecular weight and crystallinity. As is known to all, the XRD pattern of semicrystalline PET would show a lot of peaks (JCPDS, 50-2275), while the most characteristic peaks are those at $2\theta = 16.306°$, 17.745°, 21.464°, 22.725°, 24.121°, 24.967°, 26.114°, and 28.150° corresponding to the $(0\bar{1}1)$, (010), $(\bar{1}11)$, $(\bar{1}10)$, (011), $(\bar{1}12)$, (100), and $(1\bar{1}1)$ refraction, respectively. However, the XRD pattern presented in Fig. 5 shows just a broad band, indicating an amorphous material of PET-grafted-silica nanocomposites. Moreover, the molecular weight of grafted PET discussed below is low. Therefore, silica should play a role as multifunctional agents. The introduction of silica in the polymerization would lead to the interparticle or intraparticle chains to crosslink lightly. Bikiaris et al. [25] investigated the solid-state polycondensation (SSP) of the PET/silica prepolymer and found that silica particles could act as multifunctional agents to create some kind of branched or crosslinked macromolecular

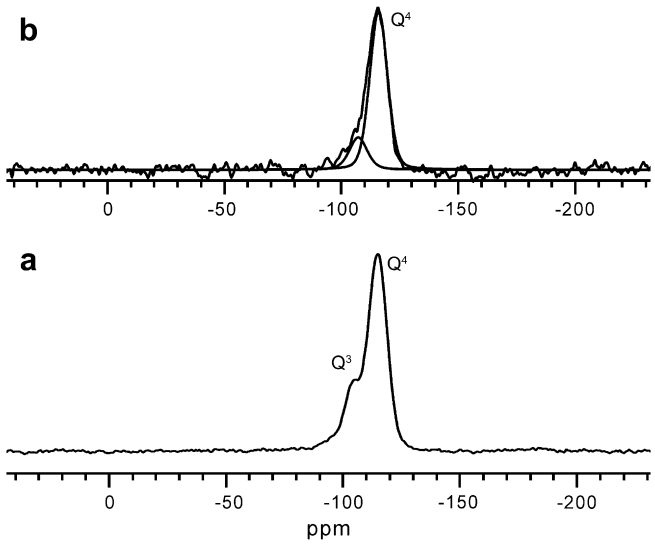

Fig. 2. ^{29}Si SPE MAS NMR spectra of (a) silica and (b) PET-grafted-silica nanocomposites.

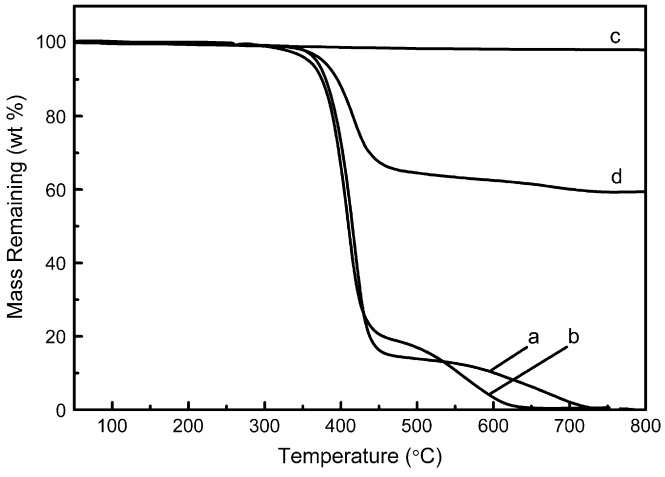

Fig. 3. Thermogravimetric analysis of (a) pure PET, (b) grafted PET, (c) silica and (d) PET-grafted-silica nanocomposites.

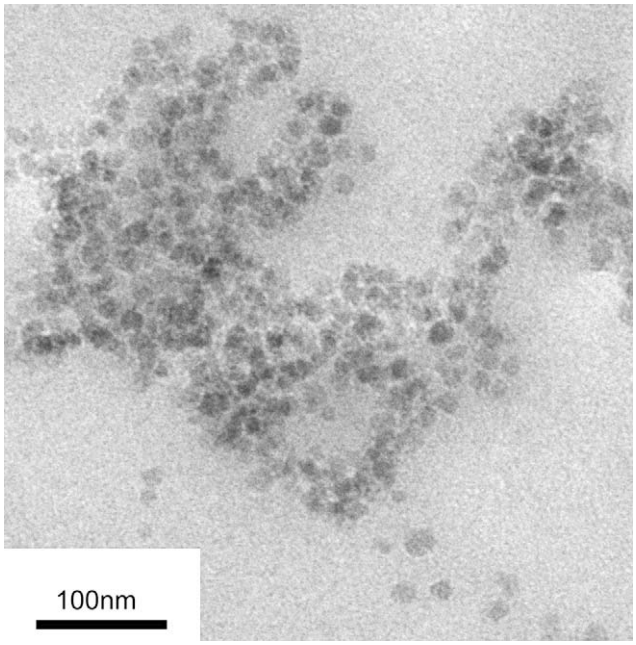

Fig. 4. TEM micrograph of PET-grafted-silica nanocomposites.

species when the silica amount was up to 5 wt%. However, with respect to PET/2 wt% silica nanocomposites in the present study, the extent of polymerization was below the point for the formation of an 'insoluble residue'. A detailed study on SSP of PET/silica nanocomposites is being studied.

To determine the molecular weight and the molecular weight distribution of grafted PET, PET-grafted-silica nanocomposites were treated with 5% aqueous hydrogen fluoride solution to etch the silica cores. Fig. 3b shows TGA curve for grafted PET. It can be seen that the weight loss of grafted PET reaches 100% at 800 °C, which indicates that the silica cores of PET-grafted-silica nanocomposites are totally etched by 5% aqueous hydrogen fluoride solution. Subsequently, we examined the effect of hydrogen fluoride solution on PET chains. Pure PET was treated with hydrogen fluoride solution under the same conditions. GPC measurements show that the molecular weight and the molecular weight distribution of the pure PET slightly change before and after the treatment of hydrogen fluoride within experimental error. This clearly indicates that hydrogen fluoride does not have effect on PET structure.

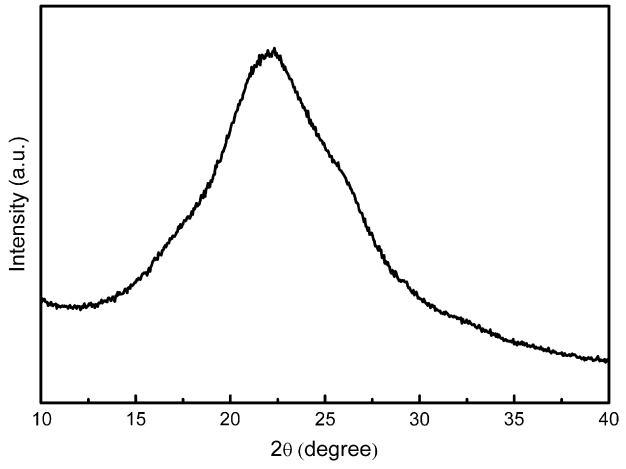

Fig. 5. XRD pattern of PET-grafted-silica nanocomposites.

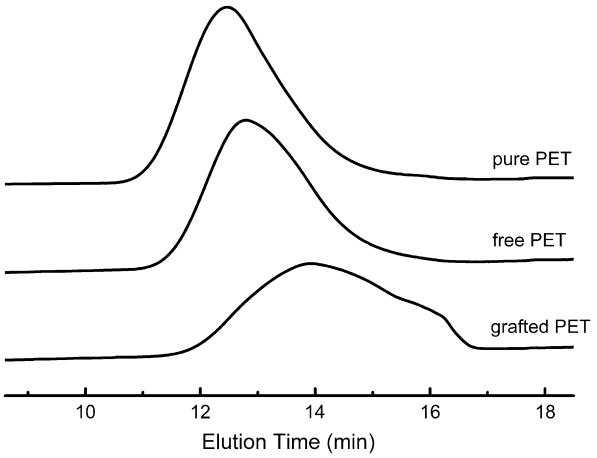

Fig. 6. GPC traces of pure PET, free PET and grafted PET.

The GPC traces of pure PET, free PET and grafted PET are depicted in Fig. 6. The molecular weight and the molecular weight distribution calculated from the GPC traces with the calibration curve for polystyrene standards are summarized in Table 2. Clearly, the molecular weight of grafted PET is much lower than that of free PET and the former has a broader molecular weight distribution. Zhou et al. [49] reported that free polymer chains with much higher molecular weight are resulted in the grafting of styrene on clay surfaces due to the limited diffusion of monomer to activated sites inside interlayers. In the present study, PET chains on silica surface have low molecular weight. It is known that the PET chains grow from the two end groups during polycondensation. However, in the case of grafted PET chains, one end group is covalently attached to the silica surface and the chain only grows from the other end. That is the main reason for the formation of low molecular weight grafted PET. Another reason is that covalent attachment of PET chains to the surfaces of silica decreases the mobility of reactive end groups, which reduces the opportunity to react and results in low molecular weight grafted PET. Moreover, the formation of lightly crosslinking structure between PET chains and silica can also restrain the growth of PET chains.

In addition, bimodal distributions were observed in the GPC trace of grafted PET. In an in situ polymerization of PET/silica nanocomposites, four reaction modes are possible. First is the condensation reaction between PET prepolymer chains to give free PET in the melt (Scheme 1a). The second is a chain propagation reaction of chemically attached PET chains on the surface of silica reacting with PET prepolymer in melt to give the hybrid nanoparticles composed of a silica core surrounded by PET chains as branches (Scheme 1b). The other two reaction modes are chain termination reactions between chemically attached PET chains on the same particle surface (Scheme 1c, intraparticle) or different particle surfaces (Scheme 1d, interparticle) to form lightly crosslinking structure, which would result in low molecular weight grafted PET on the silica surface or between silica surfaces. In this case, one can assign presumably the high-M_w peak of the GPC trace to the PET cleaved from the hybrid nanoparticles formed in the second reaction mode

Table 2
Summary of GPC results for pure PET, free PET and grafted PET.

Samples	Pure PET	PET/2 wt% silica nanocomposites	
		Free PET	Grafted PET
M_n	30 092	22 626	6468
Molecular weight distribution (M_w/M_n)	1.804	1.923	2.732

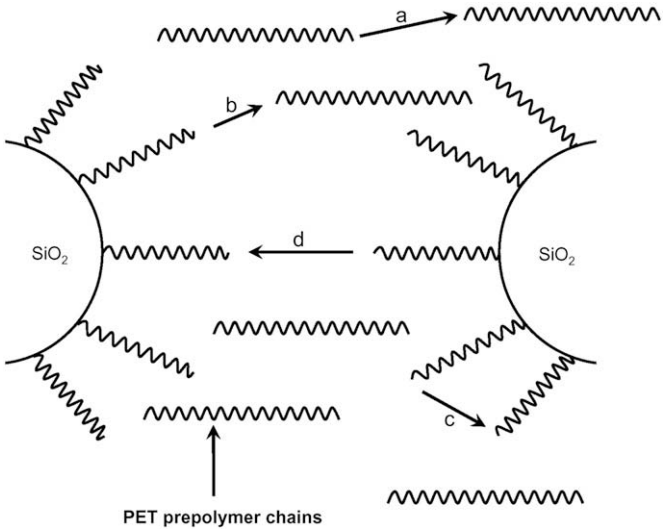

Scheme 1. Scheme of the possible reaction modes for the in situ polymerization of PET/silica nanocomposites: (a) condensation reaction to give free PET in the melt, (b) chain propagation reaction to form branched structure on the surface of silica and (c) intraparticle or (d) interparticle termination reactions to form lightly crosslinking structure.

and the low-M_w peak to the PET cleaved from the hybrid nanoparticles formed in the later two reaction modes. Complementary LLS measurements were performed to further understand the component of grafted PET. The hydrodynamic radius distribution of grafted PET was determined by dynamic light scattering (Fig. 7). It can be seen that $f(R_h)$ shows two peaks located at around 4 nm (labeled as Peak 1) and 90 nm (labeled as Peak 2), which is reasonable agreement with the GPC results and also indicates that there are two components in grafted PET. Considering the average size of the two peaks, Peak 1 could be related to the grafted PET chains corresponding to the low-M_w peak in the GPC trace, whereas Peak 2 was ascribed to a multichain one of the grafted PET chains corresponding to the high-M_w peak in the GPC trace. Based on the discussion above, a schematic diagram of the structure of PET-grafted-silica nanocomposites is given in Scheme 2.

Among the pure PET, free PET and grafted PET, the pure PET shows the highest molecular weight. The polycondensation was stopped at the same power required to agitate [39], indicating the same shear viscosity at the same shear rate. Rheology of both polymers and their

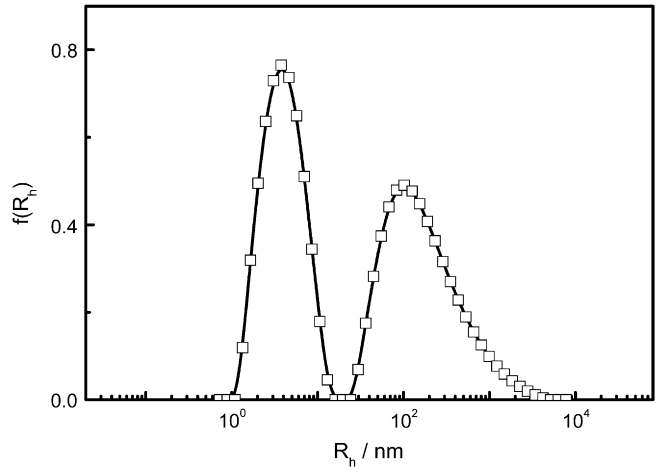

Fig. 7. The hydrodynamic radius distribution $f(R_h)$ of grafted PET by dynamic light scattering.

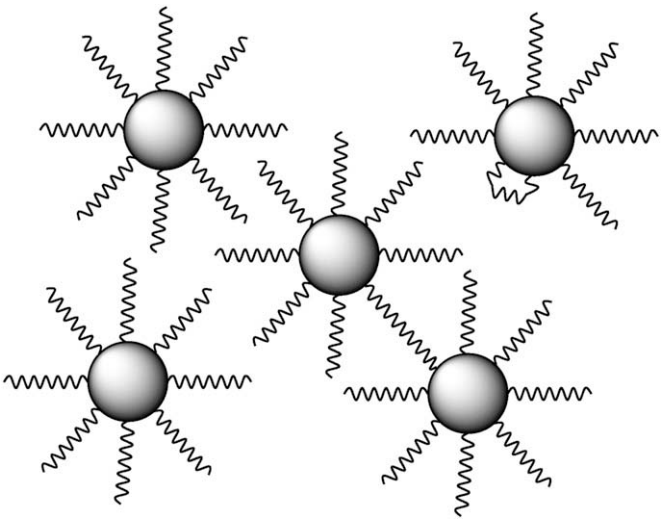

Scheme 2. Schematic diagram of the structure of PET-grafted-silica nanocomposites.

nanocomposites has been widely investigated in recent years [50–55]. The frequency dependence of the shear storage modulus (G'), loss modulus (G'') and complex viscosity (η^*) are shown in Fig. 8. Compared to pure PET, PET/2 wt%SiO_2 nanocomposites show enhancements of G', G'' and η^* over the whole frequency range, which might be due to the formation of branched and lightly

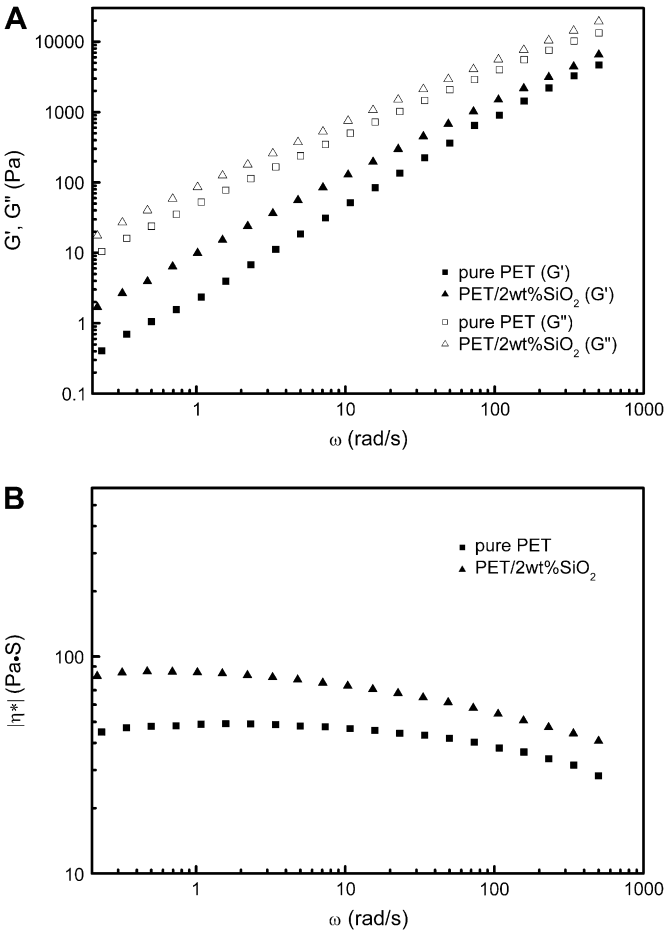

Fig. 8. Storage modulus, loss modulus (A) and complex viscosities (B) for PET and PET/2 wt% silica nanocomposites with respect to frequency.

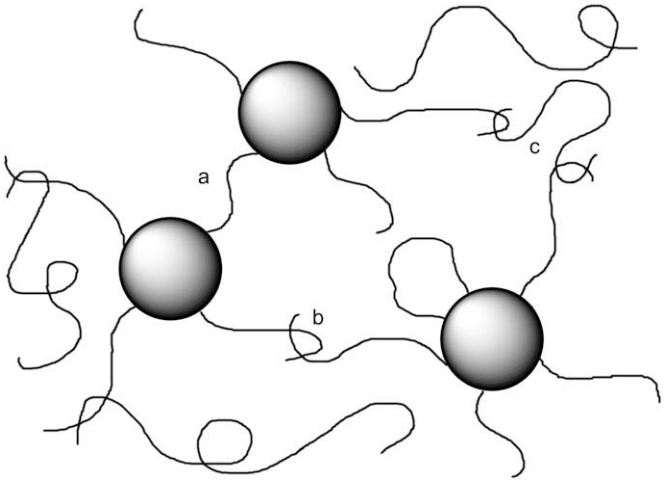

Scheme 3. Sketch map of different types of silica–PET interaction that lead to entanglement network.

crosslinking structure between PET chains and silica and the interaction of an entanglement network with silica surface. Aranguren et al. [56] investigated the rheological properties of polydimethylsiloxane filled with fumed silica and developed a model which could qualitatively relate the morphology of silica–polydimethylsiloxane suspensions with both the observed dynamic and steady shear rheological responses. Based on the structure discussed above, a model has also been developed to elucidate the interaction of an entanglement network between silica and PET chains which can be identified to three types: (1) direct bridge due to the lightly crosslinking structure between PET chains and silica (Scheme 3a); (2) primary entanglement due to branched structure between PET chains and silica (Scheme 3b); and (3) secondary entanglement involving free PET chains (Scheme 3c). The primary and secondary entanglements could be collapsed by shear force, so these enhancements weakened at higher frequency. However, the PET/2 wt% silica nanocomposites do not exhibit a typical low-frequency plateau as reported by Aranguren [56] and Jin [57], which can be attributed to two reasons: one is the reactions between PET and silica lead to a reduction of silica–silica interaction; the other is the interaction of an entanglement network is not strong enough to form a low-frequency plateau at very small concentration of silica.

4. Conclusion

The interface structure of the PET/silica nanocomposites was investigated. During the polymerization, TPA and EG firstly reacted with the silanol groups on the surface of silica to form PET-grafted-silica nanocomposites by condensation polymerization. Analysis of the chemical structure of PET-grafted-silica nanocomposites indicated formation of branched and lightly crosslinking structures between PET chains and silica. And a much lower molecular weight and broader molecular weight distribution grafted PET was resulted. The improvement in the G', G'' and η^* values of PET/2 wt% silica nanocomposites could be attributed to the interaction of an entanglement network with silica surface. Moreover, a systematic investigation on the kinetic aspect of free PET chains and grafted PET chains growing from the surface will be given in an upcoming paper.

Acknowledgements

This work is supported by National Supporting Project (2007BAE22B03), Program of Ningbo Natural Science Foundation (2006A610067) and Key program of Ningbo Industrial Science and Technology (2006B100062).

References

[1] Pyun J, Kowalewski T, Matyjaszewski K. Macromol Rapid Commun 2003;24(18):1043–59.
[2] Kickelbick G. Prog Polym Sci 2003;28(1):83–114.
[3] MacLachlan MJ, Manners I, Ozin GA. Adv Mater 2000;12(9):675–81.
[4] Chen HB, Wang MZ, Lin Y, Chan CM, Wu JS. J Appl Polym Sci 2007;106(5):3409–16.
[5] Chan CM, Wu JS, Li JX, Cheung YK. Polymer 2002;43(10):2981–92.
[6] Tsujii Y, Ohno K, Yamamoto S, Goto A, Fukuda T. Adv Polym Sci 2006;197:1–45.
[7] Brittain WJ, Boyes SG, Granville AM, Baum M, Mirous BK, Akgun B, et al. Adv Polym Sci 2006;198:125–47.
[8] Feng JT, Cai W, Sui JH, Li ZG, Wan JQ, Chakoli AN. Polymer 2008;49(23):4989–94.
[9] Wang WS, Chen HS, Wu YW, Tsai TY, Chen-Yang YW. Polymer 2008;49(22):4826–36.
[10] Lei ZQ, Wen SX. Eur Polym J 2008;44(9):2845–9.
[11] Peleshanko S, Tsukruk VV. Prog Polym Sci 2008;33(5):523–80.
[12] Zhao HY, Kang XL, Liu L. Macromolecules 2005;38(26):10619–22.
[13] An L, Pan YZ, Shen XW, Lu HB, Yang YL. J Mater Chem 2008;18(41):4928–41.
[14] von Werne T, Patten TE. J Am Chem Soc 2001;123(31):7497–505.
[15] Bartholome C, Beyou E, Bourgeat-Lami E, Chaumont P, Zydowicz N. Macromolecules 2003;36(21):7946–52.
[16] Prucker O, Ruhe J. Macromolecules 1998;31(3):592–601.
[17] Parvole J, Laruelle G, Guimon C, Francois J, Billon L. Macromol Rapid Commun 2003;24(18):1074–8.
[18] Li CZ, Benicewicz BC. Macromolecules 2005;38(14):5929–36.
[19] Pyun J, Matyjaszewski K, Kowalewski T, Savin D, Patterson G, Kickelbick G, et al. J Am Chem Soc 2001;123(38):9445–6.
[20] Mori H, Seng DC, Zhang MF, Muller AHE. Langmuir 2002;18(9):3682–93.
[21] Li DJ, Sheng X, Zhao B. J Am Chem Soc 2005;127(17):6248–56.
[22] Li C, Han J, Ryu CY, Benicewicz BC. Macromolecules 2006;39(9):3175–83.
[23] Perruchot C, Khan MA, Kamitsi A, Armes SP, von Werne T, Patten TE. Langmuir 2001;17(15):4479–81.
[24] Che JF, Luan BY, Yang XJ, Lu LD, Wang X. Mater Lett 2005;59(13):1603–9.
[25] Bikiaris D, Karavelidis V, Karayannidis G. Macromol Rapid Commun 2006;27(15):1199–205.
[26] Zhao CG, Hu GJ, Justice R, Schaefer DW, Zhang SM, Yang MS, et al. Polymer 2005;46(14):5125–32.
[27] Chen GM, Ma YM, Qi ZN. Scr Mater 2001;44(1):125–8.
[28] Chen GM, Ma YM, Qi ZN. J Appl Polym Sci 2000;77(10):2201–5.
[29] Chen GM, Liu SH, Chen SJ, Qi ZN. Macromol Chem Phys 2001;202(7):1189–93.
[30] iong LJ, Hu XB, Liu XX, Tong Z. Polymer 2008;49(23):5064–71.
[31] Halbach TS, Mulhaupt R. Polymer 2008;49(4):867–76.
[32] Sun HZ, Yang B. Sci China Ser E 2008;51(11):1886–901.
[33] Chang JH, An YU, Kim SJ, Im S. Polymer 2003;44(19):5655–61.
[34] Liu WT, Tian XY, Cui P, Li Y, Zheng K, Yang Y. J Appl Polym Sci 2004;91(2):1229–32.
[35] Qu MH, Wang YZ, Wang C, Ge XG, Wang DY, Zhou Q. Eur Polym J 2005;41(11):2569–74.
[36] Ke YC, Long CF, Qi ZN. J Appl Polym Sci 1999;71(7):1139–46.
[37] Guan GH, Li CC, Zhang D. J Appl Polym Sci 2005;95(6):1443–7.
[38] Di Lorenzo ML, Errico ME, Avella M. J Mater Sci 2002;37(11):2351–8.
[39] Tian XY, Zhang X, Liu WT, Zheng J, Ruan CJ, Cui P. J Macromol Sci Part B Phys 2006;45(4):507–13.
[40] Wallach ML. Makromol Chem 1967;103(1):19–26.
[41] Berne BJ, Pecora R. Dynamic light scattering. New York: Plenum Press; 1976.
[42] Chu B. Laser light scattering. 2nd ed. New York: Academic Press; 1991.
[43] Almazan-Almazan MC, Paredes JI, Perez-Mendoza M, Dominco-Garcia M, Lopez-Garzon FJ, Martinez-Alonso A, et al. J Colloid Interface Sci 2006;293(2):353–63.
[44] Cole KC, Ajji A, Pellerin E. Macromolecules 2002;35(3):770–84.
[45] Maciel GE, Sindorf DW. J Chromatogr 1981;205(2):438–43.
[46] Iler RK. The chemistry of silica: solubility, polymerization, colloid and surface properties, and biochemistry. New York: Wiley; 1979.
[47] Iler RK. Colloid chemistry of silica and silicates. Ithaca, NY: Cornell University Press; 1955.
[48] Laible R, Hamann K. Adv Colloid Interface Sci 1980;13(1–2):65–99.
[49] Zhou QY, Fan XW, Xia CJ, Mays J, Advincula R. Chem Mater 2001;13(8):2465–7.
[50] Hornsby PR. Adv Polym Sci 1999;139:155–217.
[51] Hu GJ, Zhao CG, Zhang SM, Yang MS, Wang ZG. Polymer 2006;47(1):480–8.
[52] Yau WW. Polymer 2007;48(8):2362–70.
[53] Tian JH, Yu W, Zhou CX. Polymer 2006;47(23):7962–9.
[54] Vidotti SE, Chinellato AC, Hu GH, Pessan LA. J Polym Sci Part B Polym Phys 2007;45(22):3084–91.
[55] Lim KY, Kim BC, Yoon KJ. J Polym Sci Part B Polym Phys 2002;40(22):2552–60.
[56] Aranguren MI, Mora E, DeGroot JV, Macosko CW. J Rheol 1992;36(6):1165–82.
[57] Jin SH, Yoon KH, Park YB, Bang DS. J Appl Polym Sci 2008;107(2):1163–8.